ADVANCED MATERIALS INTERFACES
www.advmatinterfaces.de

Controlled Mutual Diffusion between Fullerene and Conjugated Polymer Nanopillars in Ordered Heterojunction Solar Cells

Jongkuk Ko, Jiyun Song, Hyunsik Yoon, Taeyong Kim, Changhee Lee, Rüdiger Berger, and Kookheon Char**

A new approach is presented to control the nanomorphology of organic solar cells in a predictable, controllable, and easily-scalable way. The nanoimprint lithography (NIL) is combined with a subsequent molecular diffusion step controlled by thermal annealing. The new approach is realized by using nanointerdigitated donor–acceptor structure, consisting of poly(3-hexylthiophene-2,5-diyl) nanopillar arrays surrounded by phenyl-C61-butyric acid methyl ester. Subsequent thermal annealing leads to vertically aligned ordered quasi-bulk heterojunctions with hierarchical nanostructure. The changes are studied in nanostructural and electrical properties of the pillar samples using scanning probe microscopy. In addition, grazing-incidence small and wide angle X-ray scattering yield detailed quantitative information on the molecular- to domain-scale nanostructures. The changes in crystal size, chain orientation, and domain composition as a function of thermal anneal temperature and time are obtained. In addition, the conductive scanning force microscopy in quantitative imaging mode, applied to the pillar-based samples for the first time, allows us to establish a clear relationship between nanomorphology, nanoelectrical property, and macroscale device performance. It is believed that the NIL combined with controlled molecular diffusion is a powerful method, which could be easily extended to other materials and processes to realize a whole variety of other hierarchical nanomorphologies.

1. Introduction

The attributes of organic photovoltaics (OPVs)[1] devices are generally known as lightweight, low cost, and easily processible. Despite recent progresses in OPVs,[2–5] their applications are still limited by low power conversion efficiency (PCE) compared with the inorganic counterparts due to their inherent drawbacks of organic semiconductors such as short exciton diffusion length and low carrier mobility. Bulk heterojunction (BHJ) geometry of active layers in OPVs is envisioned to realize efficient solar cells by realizing the donor–acceptor phase separation within short exciton diffusion length (≈10 nm).[6,7] However, just spin coating of donor and acceptor mixtures is not sufficient to achieve consistent nanostructures which are interconnected to their respective electrodes with better charge extraction properties due to its random distribution. Various approaches have been suggested to control the nanomorphologies of BHJs and to obtain optimal nanostructure such as thermal[8] and solvent[9] annealing, solvent selection,[10] mixed solvents,[11] and using additives.[12] However, slight changes in process conditions lead to disturbed 3D nanophases, resulting in unpredictable and unscalable BHJ morphology under mass fabrication conditions. In addition, it is difficult to control the molecular-scale structures such as chain orientation and crystallinity without altering the molecular structure.

Nanoimprint lithography (NIL) has been considered to be an effective technique to solve this problem. The molecular orientation as well as domain size could be tailored with different kinds of templates and surface treatments. Silicon molds[13–17] and anodized aluminum oxide (AAO) templates[18–23] have typically been employed to realize nanopillars with diameters ranging from 20 to 250 nm. Several studies have shown that the power conversion efficiency increases when the donor–acceptor distance approaches the exciton diffusion length.[13,15,17–21,23] In addition, it has been demonstrated that the orientation of poly(3-hexylthiophene-2,5-diyl) (P3HT) donor molecules could change from the edge-on to the face-on on substrates when they are confined

J. Ko, T. Kim, Prof. K. Char
The National Creative Research Initiative Center for Intelligent Hybrids
The WCU Program of Chemical Convergence for Energy and Environment
School of Chemical and Biological Engineering
Seoul National University
Seoul 08826, Korea
E-mail: khchar@plaza.snu.ac.kr
J. Song, Prof. C. Lee
Department of Electrical and Computer Engineering
Inter-university Semiconductor Research Center
Seoul National University
Seoul 08826, Korea
Prof. H. Yoon
Department of Chemical and Biomolecular Engineering
Seoul National University of Science and Technology
Seoul 01811, Korea
Dr. R. Berger
Max Planck Institute for Polymer Research
Ackermannweg 10, D-55128 Mainz, Germany
E-mail: berger@mpip-mainz.mpg.de

DOI: 10.1002/admi.201600264

within nanostructure.[24,25] The face-on orientation, whose π–π stacking is perpendicular to substrate, leads to one or two orders of magnitude higher carrier mobility than the edge-on orientation in the direction vertical to electrodes and it is thus beneficial for the charge extraction in organic solar cells.[14,22,23] However, it is still difficult to precisely control the domain size of donor and acceptor materials using NIL because it requires different diameters and heights of templates for every different nanostructure. Particularly, control on nanostructure with size under 20 nm is much more difficult to fabricate and often requires very expensive lithography techniques.

In this work, we suggest a new fabrication method, based on the combination of NIL with subsequent self-organization of molecules to fabricate active layers of OPVs. Herein, we combine the unique advantage of NIL allowing to generate controlled morphology with the self-organization of molecules into nm-scale domains by providing an external stimulus, which is the thermal annealing in this work. Upon thermal annealing, phenyl-C61-butyric acid methyl ester (PCBM) readily diffuses into conjugated polymer films,[26,27] typically within a few seconds, leading to the bulk heterojunction architecture.[27] Here, we demonstrate that the mutual diffusion of P3HT into PCBM, which has rarely been considered before because of its relatively lower rate, is also an important factor to be considered as well as the PCBM diffusion. These systematic mutual diffusion studies allow us to precisely control the nanostructure as well as to understand their nanostructure formation mechanism which has been difficult to elucidate using previous approaches. The controlled morphology of nanostructured P3HT:PCBM with the face-on orientation combined with the mutual diffusion of donor and acceptor molecules by thermal annealing at 150 °C exhibited a 92% increase in device performance compared to the as-cast P3HT:PCBM solar cell.

2. Results and Discussion

The procedure to fabricate P3HT nanopillar arrays, based on the soft molding pattern transfer, is illustrated in **Figure 1**a. Different sizes of P3HT nanopillars can be easily prepared by the soft molding pattern transfer method which has previously been reported.[21] Polyfluoropolyether (PFPE) replica molds with hexagonal nanopores were prepared using a two-step replication process from an AAO template. The P3HT nanopillar arrays were transferred to a target substrate after filling up the nanopores of PFPE replica molds with P3HT solutions by spin casting. We note that the transfer process is possible at low temperature (120 °C) and low pressure (≈4 bars) because of low surface energy properties of PFPE molds. We fabricated P3HT nanopillars with 75 nm in diameter and 100 nm in height, confirming the nanopillars of uniform size as shown in the scanning electron microscopy image (Figure 1b). The volume ratio of empty space to P3HT nanopillars is estimated to be 1:1 (Figure 1c). Next, we deposited PCBM on the P3HT nanopillar array by spin coating using dichloromethane (DCM) as an orthogonal solvent. Scanning

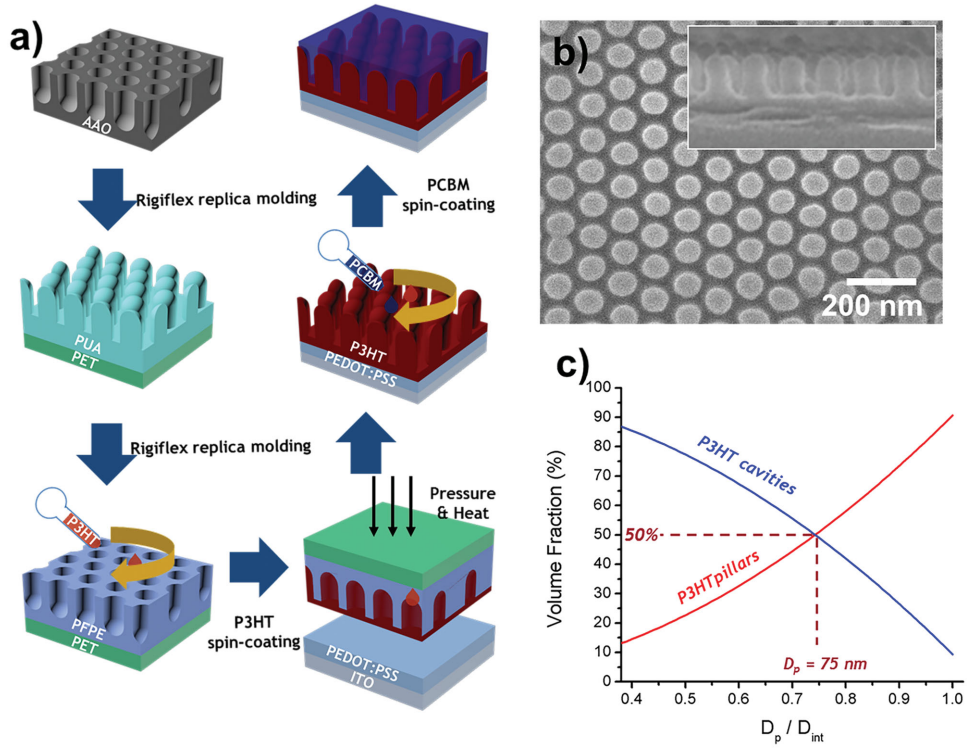

Figure 1. a) A schematic illustration for the procedure to fabricate P3HT nanopillars and subsequent PCBM deposition. b) Plan-view and cross-section scanning electron microscopy (SEM) images of P3HT nanopillars prepared. c) A diagram showing the change in volume fraction of P3HT pillars and cavities as a function of pillar diameter (where D_p is the pillar diameter and D_{int} is the pillar to pillar distance).

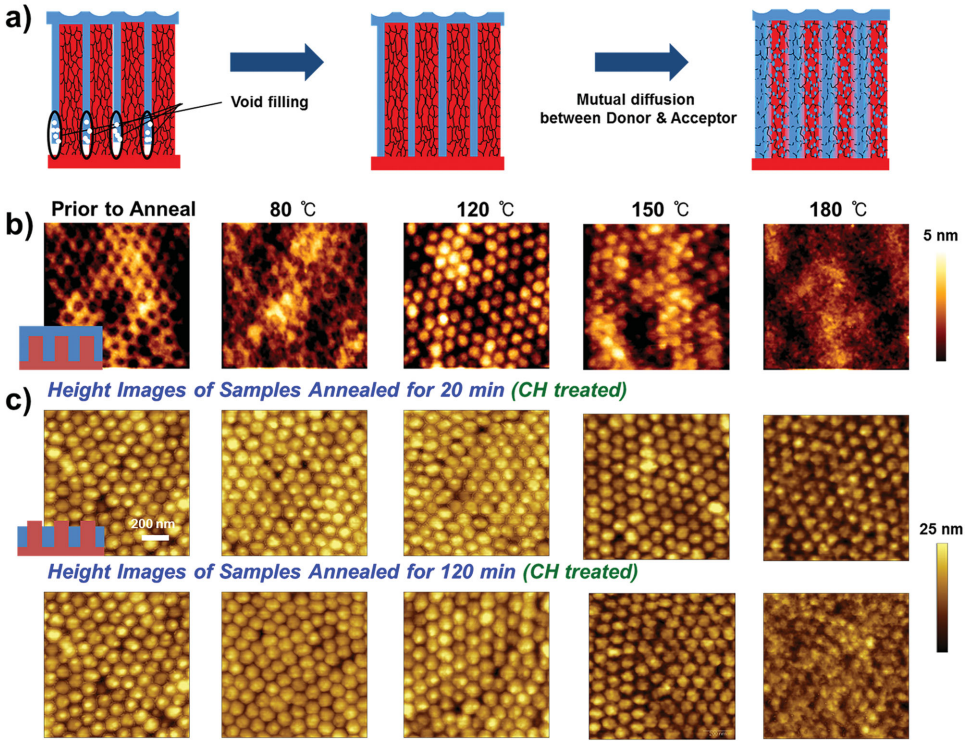

Figure 2. a) A schematic illustrating of the two types of diffusion processes. SFM height images of (b) P3HT:PCBM nanostructured samples as-prepared and annealed at four different temperatures (80, 120, 150, and 180 °C) for 20 min and c) P3HT nanopillar structures with PCBM top layers that were removed by cyclohexane.

force microscopy (SFM) analysis of the PCBM-coated samples at this process step revealed that PCBM completely covered the P3HT nanopillars (**Figure 2**b). The dimples in the topography were found at the top of the nanopillars and were attributed to voids formed during spin casting (left side of Figure 2a). Furthermore, defect areas such as delaminated P3HT pillars were not observed, indicating that the nanopillar structure was intact during sample preparation. In addition, we confirmed that our P3HT:PCBM nanostructured films were fabricated in large area with good ordering, as evidenced from grazing-incidence small angle X-ray scattering (GISAXS) measurements (Figure S1, Supporting Information).

2.1. Controlling Molecular Diffusion of Donor and Acceptor Molecules

Although the NIL is the method capable of realizing micro- to nanoscale patterns, the fabricated nanopillars of 75 nm in diameter and 100 nm in height are not sufficient to meet the requirements for perfect ordered heterojunctions (OHJs) of active layers in organic solar cells. The exciton diffusion in heterojuctions requires a distance between donors and acceptors in the range of 10 nm. Therefore, additional thermal annealing was employed to enable molecular diffusion to meet such a requirement. To explore the effect of temperature on diffusivity, SFM experiments have been performed on the patterned P3HT:PCBM thin films which were annealed for 20 min at a series of temperature from 80 to 180 °C. In addition, we soaked the samples in cyclohexane (CH) to selectively remove the upper layer of PCBM deposited on the P3HT nanopillars so that the pillar structures underneath, depending on anneal conditions, can be studied in more detail. CH has typically been used to remove top PCBM layer without affecting the P3HT layer underneath.[28] Figure 2b shows the SFM height images just after annealing the samples and Figure 2c shows the height images after soaked with cyclohexane. For the samples as-prepared and annealed at 80 °C, we noticed that there is a conversion from dimples of about 3 nm deep, located at the top of P3HT nanopillers, to small protrusions upon cyclohexane treatment observed between nontreated and CH-treated samples. We further observed that for the samples annealed at 120 and 150 °C, the small dimples observed on top of P3HT pillars become small protrusions of about 3 nm in height even without cyclohexane treatment. We attribute the conversion of the dimples to the small protrusions located on top of P3HT pillars to the decrease in the thickness of PCBM overlayer due to the migration of PCBM molecules to fill up the voids between P3HT nanopillars, as sketched in Figure 2a. Upon annealing the samples to 150 °C, the interfaces between pillars and their surroundings become fuzzy or blurry, implying that the P3HT chains mutually diffuse into the PCBM surroundings. Further increase in the anneal temperature up to 180 °C leads to the disappearance of pillar structure. We attribute the disappearance of the pillar nanostructure as the consequences of massive mutual diffusion between PCBM and P3HT molecules.

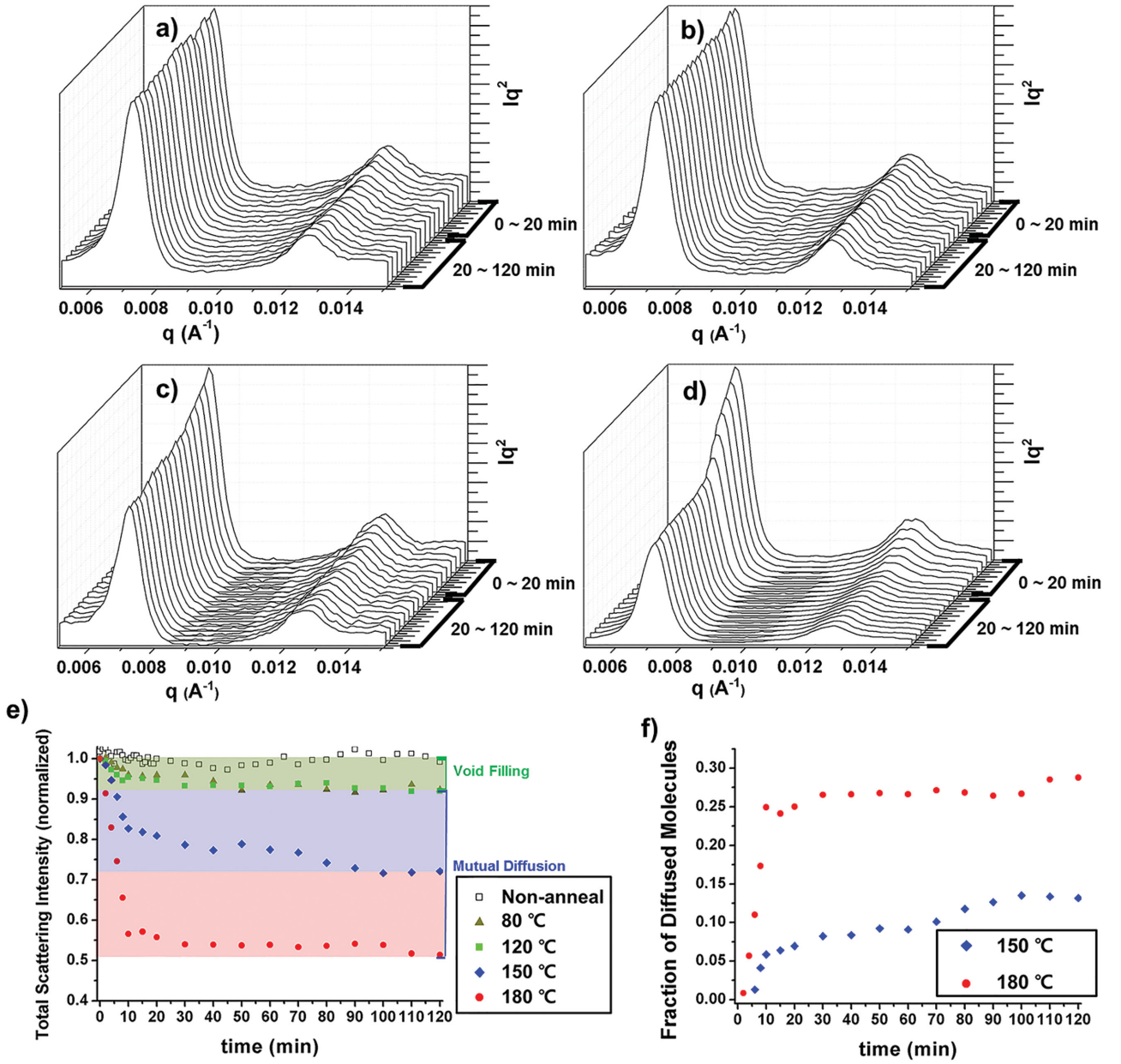

Figure 3. The changes in GISAXS scattering profiles of nanostructured P3HT/PCBM as a function of annealing time (up to 120 min) at: a) 80 °C, b) 120 °C, c) 150 °C, and d) 180 °C. e) The changes in TSI as a function of annealing time at four different anneal temperatures. f) The changes in the fraction of P3HT diffused into surroundings as a function of annealing time for the samples annealed at 150 and 180 °C.

2.2. Effect of Molecular Diffusion on Nanostructures Monitored by Grazing Incidence X-Ray Scattering

Interdiffusion of PCBM and P3HT molecules has been typically studied on bilayer systems (i.e., thin layers of P3HT placed on top of PCBM layers) using characterization tools such as dynamic Secondary Ion Mass Spectroscopy (dSIMS) and neutron reflectivity (NR).[26,27,29,30] Those previous studies reported the fast movement of PCBM into amorphous P3HT phase until they reached the equilibrium value (i.e., ≈25 wt%) when they were annealed at temperature higher than 120 °C. However, all those previous diffusion studies were based on 1D diffusion, not relevant to bulk heterojunction systems where phase-separated domains are confined in nanoscale.

GISAXS and grazing-incidence wide angle X-ray scattering (GIWAXS) measurements have been performed to quantitatively monitor the in situ molecular diffusion and its effect on pillar nanostructures. GISAXS allows us to gain information on statically averaged structures ranging from a few nanometers to several hundred nanometers, which correspond to the domain size of active layers in organic solar cells. Many investigations have previously been performed to probe the domain structures

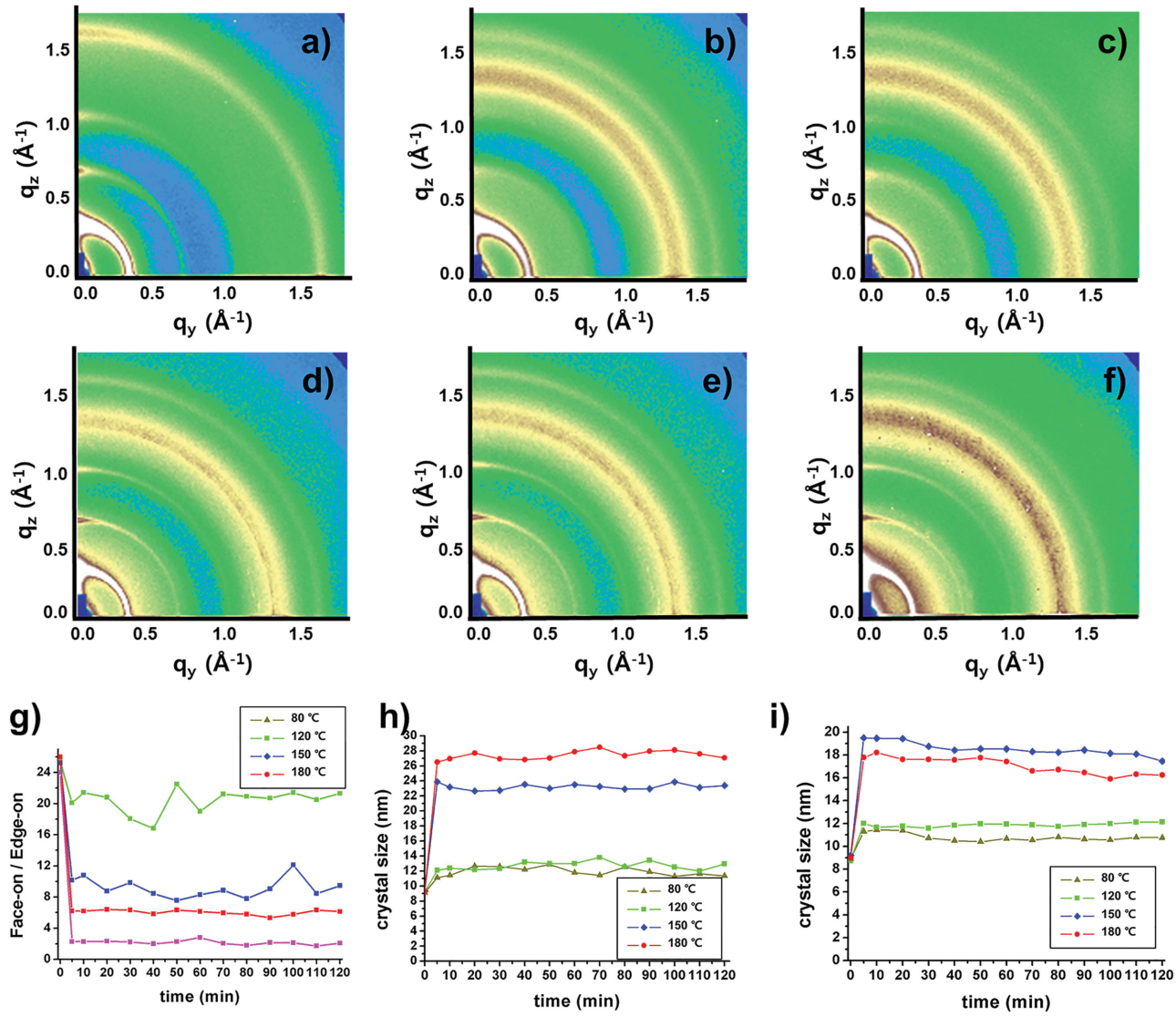

Figure 4. GIWAXS 2D scattering patterns of a) P3HT nanopillars, b) as-prepared nanostructured P3HT/PCBM films (PCBM deposited on P3HT nanopillars), and c) nanostructured P3HT/PCBM films annealed at 80 °C, d) 120 °C, e) 150 °C, and f) 180 °C. g) The ratio of face-on orientation population to edge-on orientation of nanostructured P3HT/PCBM films with four different anneal temperatures. The changes in crystal size as a function of annealing time: h) in the in-plane direction and i) in the out-of-plane direction at four different annealing temperatures.

as well as their temporal changes using in situ GISAXS.[31–33] However, since the domains in BHJs are much less ordered and polydisperse in size as well as randomly distributed in 3D, their scattering peaks are typically very weak and broadly smeared, which makes the results hard to analyze and interpret.[31] Since our hexagonally packed ordered heterojunctions with P3HT nanopillars and PCBM, produced by the new patterning approach, are well defined in large area, we could extract more information on molecular diffusion and nanostructures from pronounced higher order peaks of the hexagonal patterns. By analyzing the scattering invariants (i.e., total scattering intensities) of scattering results, two kinds of dynamic processes were also identified as already speculated in the analyses of the SFM images.

P3HT:PCBM nanostructured samples showing the first and second order scattering features correspond well with the hexagonal packing whose distance between pillars is 100 nm as shown in Figure S1 (Supporting Information). **Figure 3**a–d shows the changes in the GISAXS scattering profiles of the nanostructured P3HT/PCBM during the thermal anneal processes which induce molecular diffusion. These data clearly show the temperature- and time-dependent decrease in the scattering peaks. The amount or degree of mutual diffusion between donor and acceptor molecules can be quantitatively analyzed by calculating the total scattering intensity (TSI) of the peaks at different annealing temperatures and times. Detail equations and their calculations of TSI are described in the Supporting Information. Since we deposited PCBM on top of P3HT pillars by spin coating with DCM, we assume that a certain extent of PCBM is penetrated into the P3HT nanopillars due to partial swelling of P3HT with DCM. We thus

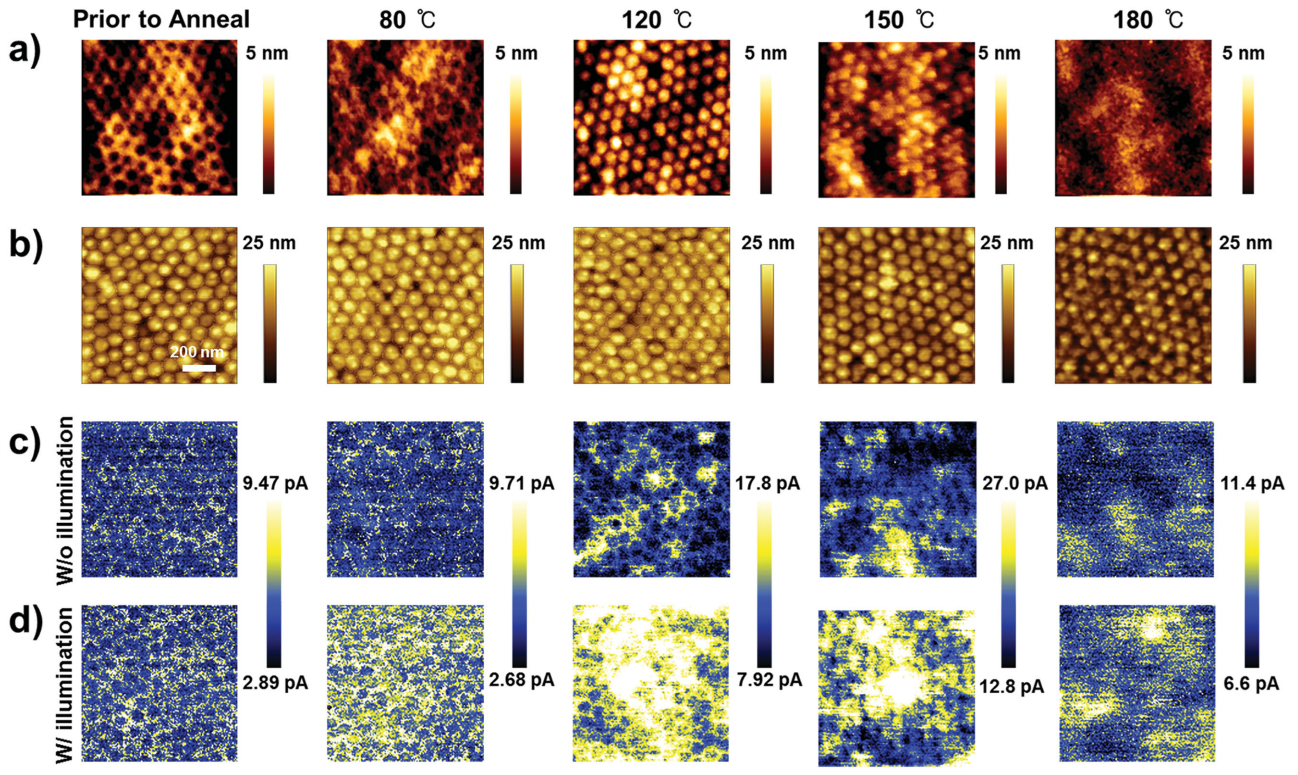

Figure 5. Height images of nanostructured P3HT/PCBM films a) with and b) without PCBM cap layer removed by cyclohexane treatment (i.e., only P3HT nanopillars remained) at four different annealing temperatures. cSFM images of nanostructured P3HT/PCBM films in the c) dark state and d) illuminated state annealed at four different temperatures.

assume that the initial states of P3HT pillars contain about 19% of PCBM which readily penetrates into the P3HT nanopillars during spin casting with DCM, based on the previous NR experiments on bilayer samples.[30] When the samples were annealed at 80 and 120 °C for 20 min, the TSI reached 96% and 94% of the initial TSI value, respectively, due to the void filling process shown in Figure 1a. Annealing at 120 °C showed a faster void filling. It reached its equilibrium TSI value of 93% within 30 min while 50 min was taken in the case of annealing the sample at 80 °C. In contrast, for the sample annealed at 150 °C, the mutual diffusion between P3HT and PCBM as well as the void filling was observed. After the void filling was complete in 4–5 min, TSI was further decreased due to the mutual diffusion between P3HT and PCBM. It reached the equilibrium value of 72% TSI, corresponding to 13% of P3HT diffused into surroundings (for detailed analysis, see Figures S3 and S4, Supporting Information). Even a faster decrease in TSI was observed when the sample was annealed at 180 °C, again due to the massive mutual diffusion, reaching their equilibrium value of 51% TSI in 30 min (corresponding to 29% of P3HT diffused into surroundings). The temperature-dependent mutual diffusion revealed by GISAXS qualitatively agrees well with the SFM results. The changes in TSI and the fractions of P3HT that diffused into the surroundings are plotted in Figure 3e,f. Current nanopillar-based OHJ systems provide ideal situations to investigate the 2D interdiffusion in nanoconfined state in more detail with useful characterization tools such as GISAXS (quantitative) and SFM (qualitative). We noted that there is a significant difference in the interdiffusion of P3HT and PCBM between unconfined bilayer diffusion couple and confined OHJ systems, emphasizing the counter diffusion of P3HT above the glass transition temperature (i.e., at 150 °C), which are more relevant to real BHJ solar cells.

GIWAXS provides information on the molecular arrangement of the crystalline phases of P3HT in terms of orientation and average size of the crystalline phases. The 2D GIWAXS patterns of imprinted P3HT nanopillars showed strong π–π peaks along the out-of-plane direction, representing the face-on orientation (**Figure 4**a). However, PCBM deposition followed by thermal annealing resulted in a slight decrease in the face-on orientation (Figure 4 and Figure S6, Supporting Information). In order to investigate the azimuthal alignment of the P3HT chains, the angular scattering profiles were obtained at the (010) peak position (Figure S6, Supporting Information). These profiles provide information on the angular distribution of π–π stacks of P3HT. Our measurements revealed that the face-on population decreased with increasing annealing temperature (Figure 4g).

The temporal changes of the P3HT (100) peaks allow determining the size of lamellae crystals during annealing at different temperatures (Figure S5, Supporting Information). Using Scherrer's equation, the temporal changes in P3HT crystal size were obtained from the corresponding (100) peak

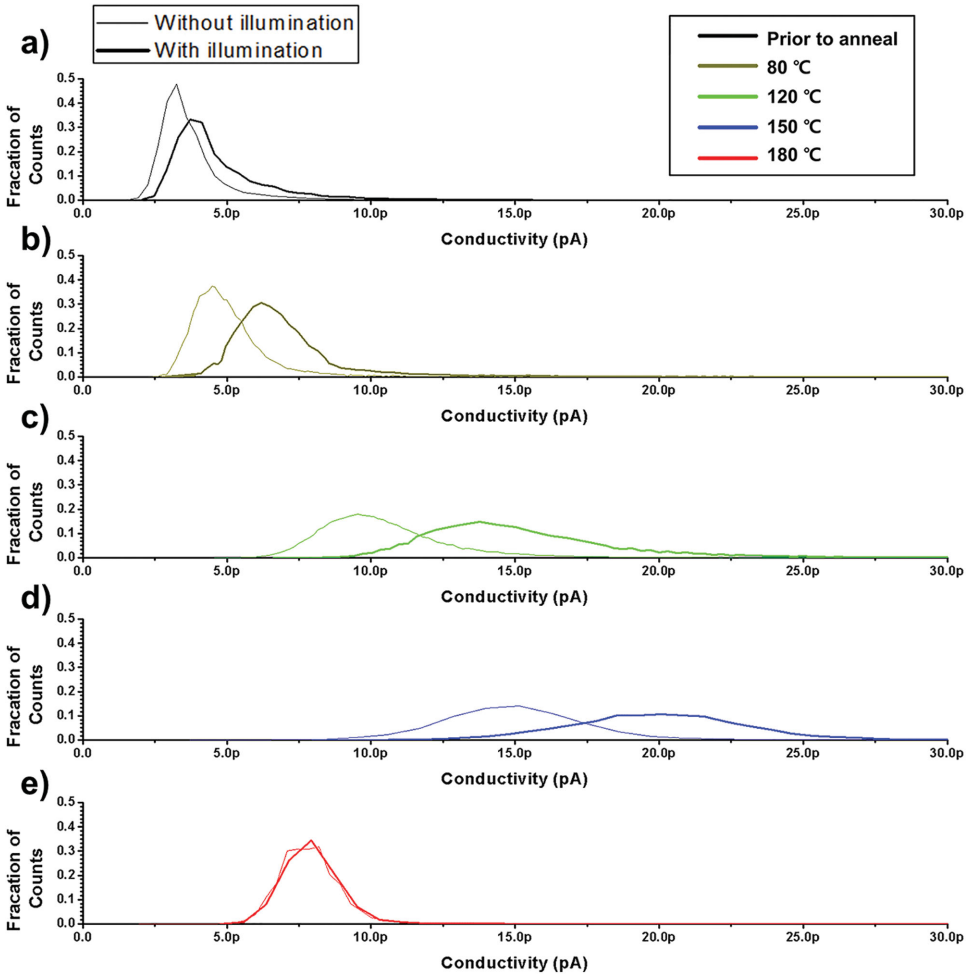

Figure 6. Histograms extracted from the cSFM results (with >1500 pillars) of Figure S8 (Supporting Information) on the nanostructured P3HT/PCBM films with (a) as prepared and annealed at: (b) 80 °C, (c) 120 °C, (d) 150 °C, and (e) 180 °C.

widths, which was extracted from the GIWAXS patterns (Figure S5, Supporting Information). The growth behaviors are shown in Figure 4h,i, showing that they reach plateau values within 5 min, which is in good agreement with the previous results.[31] As the annealing temperature was increased, the crystal size also increased. However, when the sample was annealed at 180 °C, the crystal size along the out-of-plane direction became smaller than the size annealed at 150 °C, presumably due to the nanoconfinement effects.

Table 1. Summary of ensemble average conductivity w illumination and w/o illumination extracted from the historgrams presented in Figure 6. The photoconductivity is derived from the difference of the measurements w illumination and w/o illumination.

	As-prepared	80 °C	120 °C	150 °C	180 °C
w/o illumination	3.92 pA	5.09 pA	10.5 pA	15.7 pA	8.06 pA
w/illumination	5.02 pA	7.37 pA	15.5 pA	20.4 pA	8.39 pA
Photoconductivity	1.10 pA	2.28 pA	4.95 pA	4.75 pA	0.333 pA

2.3. Relationship between Electrical Properties of Nanopillars and Device Performance

To investigate the electrical properties of individual nanopillars, we performed conductive SFM (cSFM).[34] Typically, cSFM requires contact mode operation. However, the contact mode operation on soft samples can lead to surface deformation, such that fragile polymer nanopillar structures can be easily bent or even destroyed.[19,23] To reduce or minimize this deleterious effect, a new cSFM mode has recently been developed, which is based on the torsion mode[35,36] and/or on the peak force. Here, we applied the quantitative imaging (QI) mode,[37] which allowed us to correlate the current flow between a tip and a sample at a defined loading force. First, the as-cast nanostructured P3HT/PCBM sample was investigated by QI-cSFM. For this sample, the PCBM surrounding area exhibited higher conductance when compared with the P3HT pillars upon measurements in dark and under illumination (**Figure 5**). The higher conductance is a consequence of higher charge mobility of PCBM compared to the P3HT pillars (Figure S7, Supporting Information). Annealing the samples at 80 and 120 °C, the

mean conductance as well as photoconductivity increased. We attribute this increase in photoconductivity to the decrease in void space, which leads to better contacts between electron donor and acceptor materials. Furthermore, at 80 °C we also observed that the P3HT crystal size increased even though the fraction of the face-on orientation was slightly decreased. When the sample was annealed at 150 °C, it showed the highest conductance and photoconductivity. A further increase in the annealing temperature to 180 °C resulted in the precipitous decrease in both conductance and photoconductivity down to the magnitudes of the as-cast sample. The latter result seems plausible because an annealing temperature above 150 °C leads to the destruction of percolated pathways in nanopillars and, at the same time, to the decrease in the fraction of face-on P3HT orientation. In order to obtain more statistically averaged information of the samples, we performed measurements on larger areas of 4 μm × 4 μm (Figure S8, Supporting Information). These areas correspond to the measurements of conductivities on more than 1500 nanopillars. We plotted all current values measured at each pixel of the image in the histograms (**Figure 6**). Then, we extracted the average conductivity and photoconductivity from the histograms and summarizes them in **Table 1**. The different histograms reflect higher (photo)conductivity for a proper amount of face-on orientation of P3HT pillars combined with increased crystal size.

We have so far investigated the nanomorphologies, electrical properties, and their correlations in the pillar-based P3HT/PCBM thin films depending on finely tuned molecular diffusion using various techniques such as SFM, GISAXS, GIWAXS, and QI-cSFM. To further explore the morphological and electrical effects of individual pillars on overall solar cell device performance, solar cell devices (3 mm × 3 mm) were fabricated and measured under the air mass (AM) 1.5G 1 Sun solar illumination **(Figure 7)**. Solar cell parameters deduced from current density (*J*)–voltage (*V*) curves are summarized in **Table 2**. As consistent with our results on individual pillars from QI-cSFM, different anneal conditions resulted in different short circuit current density (J_{SC}). The device performance

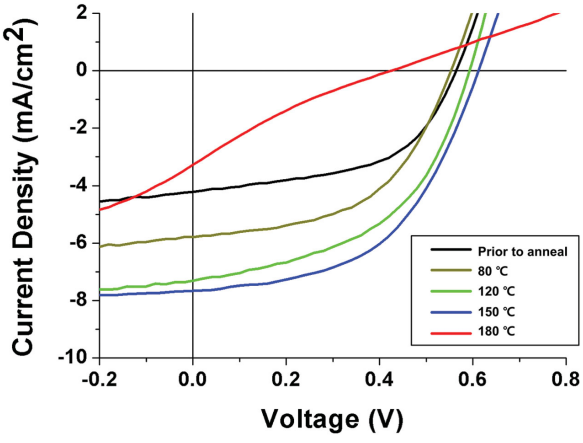

Figure 7. *J–V* characteristics of nanostructured P3HT/PCBM solar cells in different anneal conditions (as-prepared, annealed at 80, 120, 150, and 180 °C), measured under 1 Sun illumination.

Table 2. Performance parameters of nanostructured P3HT/PCBM solar cells extracted from the *J–V* characteristics.

	As-prepared	80 °C	120 °C	150 °C	180 °C
J_{SC} [mA cm^{-2}]	4.22	5.79	7.32	7.68	3.27
V_{OC} [V]	0.56	0.55	0.59	0.61	0.43
Fill Factor (FF) [%]	53.40	52.07	49.17	51.84	19.86
PCE [%]	1.27	1.67	2.13	2.44	0.28

gradually improved when the samples were annealed up to 150 °C, at which the solar cell showed 2.44% of PCE. The increase in PCE from the as-cast device to the devices annealed up to 120 °C is mainly attributed to the increase in J_{SC} because the voids initially formed at the interfaces between donor pillars and acceptor molecules disappeared upon annealing at relatively low temperature. Further increase in the device PCE with annealing the device at 150 °C is believed to originate from the additional mutual diffusion, which further reduces the pillar domain size, presumably providing more interfacial area for exciton dissociation or carrier collection. However, after annealing the solar cell device at 180 °C, the PCE dramatically decreased. At this anneal temperature, the massive mutual diffusion between P3HT and PCBM completely destroyed the imprinted percolating pathways of the P3HT pillars. In addition, we confirmed the lower fraction of face-on oriented P3HT molecules at this anneal temperature.

3. Conclusion

Nanopillar-based organic solar cells and their nanomorphology control were realized with the multistep NIL combined with mutual diffusion at different annealing temperatures. We initially fixed the volume fraction of each component (i.e., P3HT or PCBM) to be around 50% with P3HT nanopillars of an initial size of 75 nm. The P3HT pillar domain size was further reduced (or, in other words, the interfacial area was further increased) by the mutual diffusion between P3HT and PCBM, induced by thermal annealing, to realize optimal pillar morphology for efficient exciton separation. This nanopillar-based nanostructure allowed us to systematically tune the pillar morphology as well as molecular structures (i.e., orientation and crystal size) of P3HT, monitored by SFM, GIWAXS, and GISAXS, at different annealing temperature. In addition, measurements of the (photo)conductivity of nanostructured samples using cSFM were successfully applied in the present study for the first time by employing the quantitative imaging (QI) mode. We finally establish a clear relationship between pillar-based nanomorphology and microelectrical properties (which were characterized by conductive SFM) and macrodevice performance, which we believe is not readily possible with conventional BHJ structures. We are convinced that the NIL-based patterning method combined with finely tuned mutual diffusion between component organic materials could be easily extended to other organic solar cells such as all polymer solar cells to identify the optimal nanomorphology.

4. Experimental Section

Fabrication of AAO Templates and Surface Modification: AAO templates were prepared by the two-step anodization process of high purity aluminum sheet (99.999%, Goodfellow). An aluminum sheet was electropolished in a mixture solution of perchloric acid ($HClO_4$, Aldrich) and ethanol (C_2H_5OH, Aldrich) at 20 V. The polished aluminum template was then anodized at 40 V in 0.3 M oxalic acid solution at 15 °C for 4 h. After the first anodization, the aluminum oxide film was chemically eliminated by etching in a mixture of phosphoric acid and chromic acid at 45 °C for 10 h. Finally, the second anodization was performed at the same condition as the first anodization. The depth of pores was controlled by varying the time lapse of the second anodization. Subsequently, the pore widening was performed by immersing the resulting AAO template in phosphoric acid solution (10 wt%). For the surface modification of the AAO template, it was treated with oxygen plasma in 1 scm of oxygen flow at 25 W for 3 min and immersed in a solution of 0.5 wt% 3-(aminopropyl triethoxysilane) (APTES) aqueous solution for 15 min. The APTES-treated AAO template then reacted with monoglycidyl ether-terminated polydimethylsiloxane (PDMS) at 80 °C for 4 h.

Fabrication of PFPE Replica Molds and Pattern Transfer: First, nanopillar patterned polyurethane acrylate (PUA (311RM, Minuta Tech.)) was replicated from the PDMS-grafted AAO template. The PUA replica mold was detached from the AAO template after UV precure of PUA within the AAO mold. More than 3 h of additional UV cure was performed to guarantee the complete reaction of the PUA mold. The second replica mold from the PUA mold was fabricated using PFPE. Nanopore PFPE pattern was fabricated by following the same procedure to prepare the PUA replica mold. Then, a P3HT (4002-EE, Rieke-Metals) solution in chloroform was spin coated on the PFPE replica mold to fill up the nanopores of the PFPE mold. Finally, a hexagonally packed array of P3HT nanopillars was obtained by transferring the P3HT films on a target substrate with heat (120 °C for 10 min) and pressure (≈4 bars). The PFPE mold was easily released when the treatment temperature was lowered to room temperature. Nanostructures of P3HT nanopillars were characterized with Field Emission-SEM (JSM-6701F in Seoul National University Chemical and Biological Engineering Research Facilities and JSM-6700F in the National Center for Inter-University Research Facilities of Seoul National University).

Device Fabrication and Characterization: Solar cell devices were fabricated on patterned indium tin oxide (ITO)-coated glass substrates, which were cleaned using a sequence of sonication in acetone, isopropyl alcohol, and deionized water for 15 min and subsequently dried overnight in an oven. The substrates were then subjected to 10 min UV-ozone treatment. Poly(3,4-ethylene dioxythiophene):poly(styrene sulfonate) (PEDOT:PSS, Clevios HTL solar) was then spin coated at 4000 rpm for 40 s to realize a film thickness of ≈70 nm. The resulting samples were dried for 30 min at 120 °C and subsequently taken to an inert atmosphere. In a glove box, P3HT nanopillars were transferred to the PEDOT:PSS-coated ITO substrates. $PC_{60}BM$ (Nano-C) dissolved in dichloromethane was then spin coated on the P3HT nanopillars. 0.5 nm LiF and 100 nm Al layers were then thermally evaporated under 10^{-6} Torr vacuum. After the completion of device fabrication, the devices were thermally annealed at 80, 120, 150, or 180 °C for 20 min. The active area of the solar cells given by the overlap between ITO and Al electrodes was 9 mm^2.

The current density–voltage (*J*–*V*) characteristics of the solar cell devices were measured with a source measurement unit (Keithley SMU237). The device performance was characterized under AM 1.5G solar spectrum at 1 Sun (100 mW cm^{-2}) illumination simulated by a Newport 91160A device.

Quantitative Imaging (QI)-cSFM: Nanostructured P3HT/PCBM films were prepared on bare ITO substrates. QI-cSFM was performed using a Nanowizard 3 (JPK Instruments) in Advanced QI mode. Cantilevers coated with a 25 nm thick layer of chromium and platinum iridium on both sides (PointProbe® Plus Electrostatic Force Microscopy (PPP-EFM) from Nanosensors) were used to measure the conductivity of all the samples. All the measurements were performed with a tip bias voltage of +6 V. A halogen lamp with an intensity of 45 mW cm^{-2} was employed to excite and measure the photoconductivity of the samples.

GISAXS and GIWAXS Measurements: GISAXS was performed at the 3C Beamline of the Pohang Accelerator Laboratory (PAL). The sample-detector distance was 3.950 m. X-ray with a wavelength of λ = 1.135 Å and an incident angle of 0.14° were used for the measurements. GIWAXS was performed at the 9A Beamline of the PAL. X-ray with a wavelength of λ = 1.114 Å and an incident angle of 0.14° were used for the measurements. Nanostructured samples were thermally annealed in a vacuum sample chamber and they reached the final temperatures (80, 120, 150, and 180 °C) within 1–2 min and GISAXS and GIWAXS measurements on the samples were performed at a fixed temperature for 120 min.

Supporting Information

Supporting Information is available from the Wiley Online Library or from the author.

Acknowledgements

J.K. and J.S. contributed equally to this work. This research was supported by the National Creative Research Initiative Center for Intelligent Hybrids (No. 2010-0018290), the Brain Korea Plus Program in Seoul National Univerisity Chemical Engineering, the WCU Program of Chemical Convergence for Energy and Environment (R31-10013), the Technology Development Program to Solve Climate Changes (No. NRF-2009-C1AAA001-2009-0093282), and the International Research Training Group (IRTG) Program on Self-Organized Materials for Optoelectronics (No. 2011-0032203) and funded by the National Research Foundation of Korea as well as the Deutsche Forschungsgemeinschaft (DFG, Germany). In addition, this work was supported by the Human Resources Development Program (No. 20124010203170) of the Korea Institute of Energy Technology Evaluation and Planning (KETEP) grant funded by the Ministry of Trade, Industry, and Energy. The authors also thank the Pohang Accelerator Laboratory (PAL) for assigning beam time to perform GISAXS and GIWAXS experiments on the samples described in this work.

Received: March 30, 2016
Revised: May 12, 2016
Published online: June 6, 2016

[1] G. Yu, J. Gao, J. C. Hummelen, F. Wudl, A. J. Heeger, *Science* **1995**, *270*, 1789.
[2] L. Lu, T. Xu, W. Chen, E. S. Landry, L. Yu, *Nat. Photonics* **2014**, *8*, 716.
[3] Y. Yang, W. Chen, L. Dou, W.-H. Chang, H.-S. Duan, B. Bob, G. Li, Y. Yang, *Nat. Photonics* **2015**, *9*, 190.
[4] J. You, L. Dou, K. Yoshimura, T. Kato, K. Ohya, T. Moriarty, K. Emery, C. C. Chen, J. Gao, G. Li, Y. Yang, *Nat. Commun.* **2013**, *4*, 1446.
[5] H. Zhou, Y. Zhang, C. K. Mai, S. D. Collins, G. C. Bazan, T. Q. Nguyen, A. J. Heeger, *Adv. Mater.* **2015**, *27*, 1767.
[6] X. Yang, J. Loos, S. C. Veenstra, W. J. H. Verhees, M. M. Wienk, J. M. Kroon, M. A. J. Michels, R. A. J. Janssen, *Nano Lett.* **2005**, *5*, 579.
[7] Y. Kim, S. Cook, S. M. Tuladhar, S. A. Choulis, J. Nelson, J. R. Durrant, D. D. C. Bradley, M. Giles, I. McCulloch, C.-S. Ha, M. Ree, *Nat. Mater.* **2006**, *5*, 197.
[8] F. Padinger, R. S. Rittberger, N. S. Sariciftci, *Adv. Funct. Mater.* **2003**, *13*, 85.

[9] G. Li, V. Shrotriya, J. Huang, Y. Yao, T. Moriarty, K. Emery, Y. Yang, *Nat. Mater.* **2005**, *4*, 864.
[10] S. E. Shaheen, C. J. Brabec, N. S. Sariciftci, F. Padinger, T. Fromherz, J. C. Hummelen, *Appl. Phys. Lett.* **2001**, *78*, 841.
[11] F. Zhang, K. G. Jespersen, C. Björström, M. Svensson, M. R. Andersson, V. Sundström, K. Magnusson, E. Moons, A. Yartsev, O. Inganäs, *Adv. Funct. Mater.* **2006**, *16*, 667.
[12] J. Peet, J. Y. Kim, N. E. Coates, W. L. Ma, D. Moses, A. J. Heeger, G. C. Bazan, *Nat. Mater.* **2007**, *6*, 497.
[13] M.-S. Kim, J.-S. Kim, J. C. Cho, M. Shtein, L. J. Guo, J. Kim, *Appl. Phys. Lett.* **2007**, *90*, 123113.
[14] X. He, F. Gao, G. Tu, D. Hasko, S. Huttner, U. Steiner, N. C. Greenham, R. H. Friend, W. T. Huck, *Nano Lett.* **2010**, *10*, 1302.
[15] X. He, F. Gao, G. Tu, D. G. Hasko, S. Hüttner, N. C. Greenham, U. Steiner, R. H. Friend, W. T. S. Huck, *Adv. Funct. Mater.* **2011**, *21*, 139.
[16] Y. Yang, K. Mielczarek, M. Aryal, A. Zakhidov, W. Hu, *Nanoscale* **2014**, *6*, 7576.
[17] X. Lu, H. Hlaing, C.-Y. Nam, K. G. Yager, C. T. Black, B. M. Ocko, *Chem. Mater.* **2015**, *27*, 60.
[18] N. Haberkorn, S. A. Weber, R. Berger, P. Theato, *ACS Appl. Mater. Interfaces* **2010**, *2*, 1573.
[19] J. S. Kim, Y. Park, D. Y. Lee, J. H. Lee, J. H. Park, J. K. Kim, K. Cho, *Adv. Funct. Mater.* **2010**, *20*, 540.
[20] D. Chen, W. Zhao, T. P. Russell, *ACS Nano* **2012**, *6*, 1479.
[21] T. Kim, H. Yoon, H. J. Song, N. Haberkorn, Y. Cho, S. H. Sung, C. H. Lee, K. Char, P. Theato, *Macromol. Rapid Commun.* **2012**, *33*, 2035.
[22] T. Pfadler, M. Coric, C. M. Palumbiny, A. C. Jakowetz, K.-P. Strunk, J. A. Dorman, P. Ehrenreich, C. Wang, A. Hexemer, R.-Q. Png, P/H. Ho, P. Muller-Buschbaum, J. Weickert, L. Schmidt-Mende, *ACS Nano* **2015**, *8*, 12397.
[23] G. Ding, C. Li, X. Li, Y. Wu, J. Liu, Y. Li, Z. Hu, Y. Li, *Nanoscale* **2015**, *7*, 11024.
[24] M. Aryal, K. Trivedi, W. W. Hu, *ACS Nano* **2009**, *3*, 3085.
[25] D. E. Johnston, K. G. Yager, H. Hlaing, X. Lu, B. M. Ocko, C. T. Black, *ACS Nano* **2014**, *8*, 243.
[26] D. Chen, F. Liu, C. Wang, A. Nakahara, T. P. Russell, *Nano Lett.* **2011**, *11*, 2071.
[27] N. D. Treat, M. A. Brady, G. Smith, M. F. Toney, E. J. Kramer, C. J. Hawker, M. L. Chabinyc, *Adv. Energy Mater.* **2011**, *1*, 82.
[28] A. L. Ayzner, C. J. Tassone, S. H. Tolbert, B. J. Schwartz, *J. Phys. Chem. C* **2009**, *113*, 20050.
[29] H. Chen, R. Hegde, J. Browning, M. D. Dadmun, *Phys. Chem. Chem. Phys.* **2012**, *14*, 5635.
[30] K. H. Lee, Y. Zhang, P. L. Burn, I. R. Gentle, M. James, A. Nelson, P. Meredith, *J. Mater. Chem. C* **2013**, *1*, 2593.
[31] W.-R. Wu, U.-S. Jeng, C.-J. Su, K.-H. Wei, M.-S. Su, M.-Y. Chiu, C.-Y. Chen, W.-B. Su, C.-H. Su, A.-C. Su, *ACS Nano* **2011**, *5*, 6233.
[32] K. W. Chou, B. Yan, R. Li, E. Q. Li, K. Zhao, D. H. Anjum, S. Alvarez, R. Gassaway, A. Biocca, S. T. Thoroddsen, A. Hexemer, A. Amassian, *Adv. Mater.* **2013**, *25*, 1923.
[33] S. Guo, M. A. Ruderer, M. Rawolle, V. Korstgens, C. Birkenstock, J. Perlich, P. Muller-Buschbaum, *ACS Appl. Mater. Interfaces* **2013**, *5*, 8581.
[34] R. Berger, A. L. Domanski, S. A. L. Weber, *Eur. Polym. J.* **2013**, *49*, 1907.
[35] S. A. Weber, N. Haberkorn, P. Theato, R. Berger, *Nano Lett.* **2010**, *10*, 1194.
[36] S. A. L. Weber, R. Berger, *Appl. Phys. Lett.* **2013**, *102*, 163105.
[37] H. Haschke, T. Jaehnke, *Laser Focus World* **2012**, *48*, 25.